

The Ser/Thr protein kinase PrkC imprints phenotypic memory in *Bacillus anthracis* spores by phosphorylating the glycolytic enzyme enolase

Richa Virmani^{1,2,3}, Andaleeb Sajid², Anshika Singhal², Mohita Gaur¹, Jayadev Joshi², Ankur Bothra², Richa Garg², Richa Misra^{1,6}, Vijay Pal Singh², Virginie Molle⁵, Ajay K. Goel⁴, Archana Singh², Vipin C. Kalia⁷, Jung-Kul Lee⁷, Yasha Hasija³, Gunjan Arora^{1,8*} and Yogendra Singh^{1,2*}

¹Department of Zoology, University of Delhi, Delhi 110007, India.

²CSIR- Institute of Genomics and Integrative Biology, Delhi 110007, India.

³Delhi Technological University, Delhi 110042, India.

⁴Defence Research and Development Establishment, Gwalior 474002, India.

⁵DIMNP, CNRS, University of Montpellier, Montpellier, France.

⁶Sri Venkateswara College, University of Delhi, India.

⁷Department of Chemical Engineering, Konkuk University, 1 Hwayang-Dong, Gwangjin-Gu, Seoul 05029, Republic of Korea.

⁸Laboratory of Immunogenetics, National Institute of Allergy and Infectious Diseases, National Institutes of Health, Rockville, MD 20851, USA.

Running title: *Phenotypic memory in B. anthracis*

*To whom the correspondence should be addressed: Gunjan Arora (arorag1983@gmail.com) and Yogendra Singh (ysinghdu@gmail.com)

Department of Zoology, University of Delhi, Delhi 110007, India

Keywords: *Bacillus*, signaling, spore germination, PrkC, metabolism, glycolysis, virulence, anthrax, phenotypic memory

ABSTRACT

Bacillus anthracis is the causative agent of anthrax in humans, bovine, and other animals. *B. anthracis* pathogenesis requires differentiation of dormant spores into vegetative cells. The spores inherit cellular components as phenotypic memory from the parent cell, and this memory plays a critical role in facilitating the spores' revival. Since metabolism initiates at the beginning of spore germination, here we metabolically reprogrammed *B. anthracis* cells to understand the role of glycolytic enzymes in this process. We show that increased expression of enolase (Eno) in the sporulating mother cell decreases germination efficiency. Eno is phosphorylated by the conserved Ser/Thr protein kinase PrkC and decreases the catalytic activity of Eno. We found that phosphorylation also regulates Eno expression and localization, thereby controlling the overall spore germination process. Using MS analysis, we identified the sites of phosphorylation in Eno, and substitution(s) of

selected phosphorylation sites helped establish the functional correlation between phosphorylation and Eno activity. We propose that PrkC-mediated regulation of Eno may help sporulating *B. anthracis* cells in adapting to nutrient deprivation. In summary, to the best of our knowledge, our study provides the first evidence that in sporulating *B. anthracis*, PrkC imprints phenotypic memory that facilitates the germination process.

Deciphering the role of metabolic enzymes that orchestrate morphogenic transition states in bacteria is a fundamental question. *Bacillus anthracis* is the causative agent of anthrax in human, bovine and other animals (1,2). It is known to survive hostile environments by forming spores that remain quiescent and retain minimum metabolic activity (3,4). As a pathogen, the success of *B. anthracis* depends on the spore's ability to develop into a growing vegetative cell. Under favorable conditions, spore metabolism is triggered, in order to support energy needs and to

develop into a fully functional cell (5). The metabolic checkpoints and energy reserves in the spore provide different stimuli at an early growth stage and ensure the completion of the developmental program. Therefore, the transformation of a dormant spore into a vegetative cell is a key step in the pathogenic cycle of *B. anthracis*. However, the molecular events leading to successful spore dormancy and later to germination, remain to be fully elucidated.

During the process of germination, some spores disintegrate their protective structure and grow into vegetative cells (5). Sporulating cells carry a substantial set of macromolecules (including several proteins) through their journey from progenitor cell to spore (6). The role of these proteins remains largely unknown. This carry-over of cellular components is termed ‘phenotypic memory’ (7). The efficiency of spore germination has been shown to be determined by this phenotypic memory inherited from the parent cell (7,8). In a recent study, the role of one such protein- Alanine dehydrogenase that controls alanine-induced outgrowth in cellular memory, was described (7). Since the protein cargo remains constant in the spore, these proteins decide the fate of the reviving spore depending on environmental conditions and sensory signaling molecules (9). There have been considerable efforts towards understanding the spore germination process and involvement of signaling mechanisms (10-12).

The link between metabolism and the spore revival process is not explored well. At the onset of germination, metabolism resumes without requiring new macromolecular synthesis (13). Reports in *B. subtilis* have highlighted the essentiality and interactions of glycolytic enzymes phosphofructokinase (Pfk), phosphoglyceromutase (Pgm) and enolase (Eno) (14). Eno and Pgm play an essential role in both glycolysis and gluconeogenesis, where Pgm reversibly converts 3-phosphoglyceric acid (3-PGA) to 2-PGA, and Eno catalyzes the penultimate step of glycolysis by conversion of 2-PGA to phosphoenolpyruvate (PEP), thus deciding the flux of pathway. Bacteria survive harsh conditions efficiently by keeping an alternate source of energy, 3-PGA, which is used during the early events of spore germination (15). A balanced ratio of 3-PGA and 2-PGA is maintained at the time of spore formation by keeping the spore metabolically dormant. Further, the dehydrated, acidic core of spore

diminishes the metabolic activity to maintain the 3-PGA reserve (16). Since spores of *Bacillus sp.* are known to hold significant levels of 3-PGA reserves, we decided to investigate the role of Eno in the spore germination process of *B. anthracis*. Previous studies have shown that an Eno deletion-mutant strain was defective in sporulation, while its inhibition led to a lag in ATP production during the course of germination, thus uncovering a role for Eno in the bacterial life cycle (17,18). Besides this, Eno is a component of the adsorbed anthrax vaccine and has been indicated in helping bacteria evade the innate immune cells by binding to host plasminogen (19,20).

In this study, we address the role of Eno in spore germination. Our results show that Eno acts as an intrinsic memory controller that influences the germination process and is regulated by the Ser/Thr protein kinase (STPK) PrkC.

RESULTS AND DISCUSSION

***B. anthracis* Eno influences spore germination**
In order to decipher the contribution of some key metabolic enzymes in spore germination, we cloned and expressed the glycolytic pathway genes- *pgk*, *pgm* and *eno*, that are important for maintaining the 3-PGA reserve. The *B. anthracis* Sterne (Bas) strains over-expressing (phosphoglycerate kinase) Pgk, Pgm and Eno were analyzed for their sporulation and germination efficiencies. As shown in Figure 1A, an increase in the expression of either glycolytic protein led to a decrease in sporulation efficiency. For germination efficiency, there was approximately 75% decrease in Eno over-expressing spores, while spores over-expressing Pgk and Pgm showed only about 20% and 40% decrease, respectively (Fig. 1B). To assess the levels of Eno in the overexpression strain, we generated Eno-specific polyclonal antibodies in mice (Fig. S1). Immunoblotting with these antibodies showed that the expression of Eno was increased by ~1.5-fold in the recombinant strain as compared to parent strain (Fig. S2).

Eno expression is reduced in *B. anthracis* spores
Our results suggest that overexpression of Eno causes a decrease in spore germination. Therefore, we decided to check the intrinsic regulation of Eno expression in spores as well as in vegetative cells. Using Eno-specific polyclonal antibodies, we determined the expression of Eno

in whole cell lysates at different stages of the *B. anthracis* lifecycle. The immunoblot with anti-Eno antibody detected a specific band at 45 kDa corresponding to the molecular weight of Eno. After quantification of band intensities, differential expression of Eno was observed in several growth stages relative to early log phase, where the maximum expression was observed (Fig. 2). The expression decreased in the later growth stages (log-phase, late log and stationary phase), until in a spore-forming stage only 30% of the protein remained with respect to early log phase. Since spores have lower levels of Eno as compared to vegetative cells and over-expression of Eno leads to reduced fitness of the Bas strain during spore germination, there seems to be decisive role of Eno in germination.

*Eno is phosphorylated in vitro by the *B. anthracis* STPK PrkC*

Signaling mechanisms regulate the transition of *B. anthracis* from dormancy to vegetative state (21,22). Interestingly, there is a growing body of evidence supporting the notion that PrkC could play an important role in spore's exit from dormancy (12,23,24). In our previous studies, we found that glycolytic enzymes are subjected to regulation by phosphorylation (25,26). Large scale phosphoproteome analysis in *B. subtilis* also indicates phosphorylation of Eno, which is a close homolog of *B. anthracis* Eno (~80% sequence similarity) (27). Additionally, in our previous study, comparison of phosphoproteomic analysis of *B. anthracis* wild-type (Bas-wt) and *prkC* deletion mutant (BasΔ*prkC*) identified phosphorylated isoforms of Eno (28). Therefore, we hypothesized that Eno could be regulated by PrkC-mediated phosphorylation and this regulation might be important for *B. anthracis* morphogenesis.

To address this hypothesis, *in vitro* kinase assays were performed using recombinant PrkC and Eno with [γ -³²P] ATP. As shown in Figure 3A, Eno was found to be phosphorylated by PrkC. No phospho-transfer was observed when Eno was incubated alone or with the Ser/Thr phosphatase PrpC. Phospho-transfer kinetics using *in vitro* kinase assay and 2-dimensional gel electrophoresis indicated phosphorylation of Eno at early time points (Fig. 3B, 3C and 3D). Thus, these assays confirmed that Eno is a substrate of PrkC. Subsequently, the phosphorylation of Eno was also confirmed *in vivo* using co-expression with PrkC and PrpC in *Escherichia coli*. Eno was found to be

phosphorylated when co-expressed with PrkC (Eno-P), while no phosphorylation was observed when co-expressed with PrpC, (Eno-UP) as confirmed by Pro-Q diamond phosphorylation-specific staining (Fig. 3E). Eno-P isolated from metabolically labeled cells with [³²P]-orthophosphoric acid showed ³²P-labeled Eno band, showing PrkC-specific phosphorylation under native conditions in *E. coli* (Fig. 3F).

Eno is phosphorylated on Serine and Threonine residues

To identify the residues in Eno phosphorylated by PrkC, purified Eno-P and Eno-UP proteins were subjected to mass spectrometry (Fig. S3). We found nine phosphorylated serine and threonine residues in Eno-P, while no phosphorylated residues were identified in Eno-UP. To understand the location of phosphorylation sites in Eno, we generated a homology model of *B. anthracis* Eno using the crystal structure of *B. subtilis* Eno (PDB: 4A3R) (29). Figure 4A shows the Bas-Eno homology model with the phosphorylation sites marked. Three phosphorylated residues (Ser³³⁶, Thr³⁶³ and Ser³⁶⁷) were localized in the C-terminal hydrophobic region, while the remaining six residues were present at the protein surface (Fig. 4A). Amongst these sites, Ser³⁶⁷ was highly conserved amongst the Eno homologs and was found to be present in the flexible loop responsible for catalysis, as identified by multiple sequence alignment of Eno and its homologs (Fig. S4). Previously, Eno-Ser³⁶⁷ was also identified as a phosphorylated residue in spore phosphoproteome of *B. subtilis* (27). Further structural analysis of the three C-terminal residues indicated that Ser³⁶⁷ could interact with the catalytic site residues Lys³⁴⁰ and Ile³³⁹ (Fig. 4B), while Thr³⁶³ and Ser³³⁶ were present on the parallel and antiparallel strands, stabilizing the structure of the protein (Fig. 4C).

To determine the role of individual phosphorylation sites, we chose to study the three C-terminal residues located in the hydrophobic pocket. These residues were mutated to generate single mutants Eno^{T363A}, Eno^{S336A}, Eno^{S367A}, a double mutant Eno^{S336A/T363A}, and a triple mutant Eno^{S336A/T363A/S367A}. Equal amounts of Eno and its mutant derivatives were used in *in vitro* kinase assay with PrkC. Quantification of phosphorylation levels indicated a significant decrease in signal for all the single Eno mutants while the double mutant Eno^{S336A/T363A} showed >60% loss in phosphorylation levels (Fig. 4D). In

the triple mutant ($\text{Eno}^{\text{S336A/T363A/S367A}}$), there was a significant loss (>80%) in phosphorylation (Fig. 4E), showing that Ser³³⁶, Thr³⁶³ and Ser³⁶⁷ were important phosphorylation sites.

The role of these three residues was also analyzed in regulating the enzyme activity. In glycolysis, Eno catalyzes the penultimate step by converting 2-PGA to PEP. We evaluated the phosphorylation-mediated variations on the activity of Eno by using a kit-based colorimetric assay which measures the formation of an intermediate product during this conversion. As shown in Figure 4F, a considerable loss (40-50%) in the activity of $\text{Eno}^{\text{S336A}}$ and $\text{Eno}^{\text{S367A}}$ mutants was observed, whereas $\text{Eno}^{\text{T363A}}$ exhibited an increase in activity. Further, the triple mutant showed a ~40% decrease in the overall protein activity as compared to the Eno-wt (Fig. 4G).

To understand the effect of mutations on the structural integrity of Eno, we performed circular dichroism (CD) spectroscopy using Eno purified from *E. coli* (Eno-wt), Eno-P (Eno co-expressed with PrkC), Eno-UP (Eno co-expressed with PrpC) and the triple mutant $\text{Eno}^{\text{S336A/T363A/S367A}}$. To our surprise, all four samples showed a similar alpha-helix and beta-sheet composition, suggesting that the mutations as well as phosphorylation do not affect the secondary structure of the protein and maintain overall conformation (Table 1).

Previous studies on Eno structure from diverse species have shown that Ser³⁶⁷ is a part of a flexible loop, as mentioned earlier (30). This flexible loop is involved in binding to 2-PGA and subsequent conformational change. Additionally, we found this loop to be conserved in Eno from different species (Fig. S4). Therefore, we speculate that this flexibility of the loop and associated conformational change in the absence of substrate might allow the residue to get phosphorylated by the kinase (31).

Eno is phosphorylated in *B. anthracis* vegetative cells and spores

We next investigated the *in vivo* phosphorylation status of Eno. We over-expressed Eno with a C-terminal poly-histidine tag in Bas-wt (Bas Eno) and BasΔprkC (BasΔprkC Eno) Sterne strains. Purified proteins from respective strains were subjected to immunoblotting using anti-pSer and anti-pThr antibodies. Eno-P (co-expressed with PrkC) was used as a positive control and *E. coli* Eno (not co-expressed with PrkC) was used as a negative control. pSer and pThr specific antibodies recognized Eno purified from Bas-wt,

whereas, the phosphorylation signal was significantly reduced, though not completely absent, in the BasΔprkC strain (Fig. 5A and B). This result indicates that Eno is predominantly phosphorylated by PrkC *in vivo* but may also be targeted by other kinases in absence of PrkC.

Furthermore, we analyzed the stoichiometry of *in vivo* phosphorylation of Eno by resolving the phosphorylated and unphosphorylated isoforms on 2-D gel electrophoresis. Whole cell protein extracts from Bas-wt and BasΔprkC were subjected to electrophoresis followed by immunoblotting with anti-Eno antibody. Four Eno isoforms were observed in BasΔprkC cells (Fig. 5C). However, in Bas-wt cells, we identified seven Eno isoforms among which four were present at a pI similar to that in the BasΔprkC strain (pI 4.5-5.0), while the remaining three isoforms migrated at acidic pI range (towards 4.0, Fig. 5C), thus confirming PrkC-specific phosphorylation of Eno in vegetative cells.

Next, we investigated whether Eno was phosphorylated in spores. We over-expressed and purified Eno from *B. anthracis* spore lysate (Eno Bas Spore) followed by immunoblotting with anti-pThr antibody. Eno phosphorylation was detected in spores despite its low expression (Fig. 5D). The phosphorylation was also confirmed by using anti-pSer antibodies (Fig. S5). These results show that Eno is regulated by PrkC-mediated phosphorylation in spores of *B. anthracis*, confirming its role in spore germination.

Phosphorylation decreases catalytic activity and Mg²⁺cofactor affinity of Eno

After establishing that Eno is a substrate of PrkC, we investigated the effect of phosphorylation on Eno activity. In the activity assay, Eno-P was found to be ~60% less active than Eno-UP, suggesting that phosphorylation causes a decrease in the activity of Eno (Fig. 6A).

Interestingly, spores contain high concentrations of divalent cations such as Ca²⁺, Mg²⁺ and Mn²⁺ to keep themselves dehydrated, thus maintaining a low metabolic profile (32,33). As Eno is a metalloenzyme requiring Mg²⁺ as a cofactor (34), we investigated if phosphorylation had an impact on Eno-Mg²⁺ interaction. Eno-P and Eno-UP (co-expressed with PrkC and PrpC, respectively) were used to study the phosphorylation-mediated regulation of the Eno-Mg²⁺ interaction. A fluorimetry-based method was used to measure variations in the intrinsic tryptophan fluorescence of Eno upon addition of

$MgCl_2$ (35). We observed that Eno: Mg^{2+} complex formation was correlated with an enhancement of tryptophan fluorescence intensity. Our data showed that fluorescence of Eno-UP with Mg^{2+} was higher than that of Eno-P, indicating a negative effect of phosphorylation on metal binding (Fig. 6B). Different concentrations of Mg^{2+} were titrated with Eno-UP or Eno-P and the binding constant (K_a) was calculated. For Eno-UP, the K_a was higher (0.254 ± 0.01 M) than the K_a for Eno-P (0.181 ± 0.03 M). Hence, these results show that Eno phosphorylation reduces Mg^{2+} binding affinity, which is in agreement with the decreased activity of phosphorylated Eno.

PrkC is involved in the regulation of Eno expression in spores

We further analyzed the effect of Eno phosphorylation on its expression in spores by comparing the protein levels of Eno in spores of Bas-wt and Bas Δ prkC Sterne strains (Fig. 7A), as well as during exponential growth (Fig. 7B). Our results showed 2 to 3-fold higher protein levels of Eno in Bas Δ prkC spores compared to Bas-wt spores, while the expression was similar in both strains during the exponential phase (Fig. 7 and S6). Thus, Eno protein levels might be regulated by PrkC. These results could in part explain the compromised virulence phenotype of the PrkC null mutant as observed in earlier studies (36). However, it remains to be determined if this PrkC-dependent regulation is direct or indirect. It could be hypothesized that PrkC phosphorylates a yet to be discovered transcription factor that regulates the expression of Eno. Such regulation could occur upon a signal received by PrkC at the onset of sporulation to trigger Eno down-regulation.

Eno phosphorylation status does not regulate its secretion but may affect its cellular localization

Surface-exposed signaling proteins like PrkC might be involved in maintaining the cellular dynamics during morphogenesis by modifying the activities and localization of metabolic enzymes to fulfill cellular requirements. Therefore, we examined if the phosphorylation status of Eno could be linked to its cellular localization. To find the localization of Eno within the vegetative cells, we probed the native protein in Bas-wt cells in exponential phase by anti-Eno antibodies using immuno-Electron Microscopy (EM). Eno was found to be localized at the cell membrane and cytoplasm (Fig. 8A, B

and S7). Subsequently, we compared the localization of Eno in Bas Δ prkC and prkC-complement strains at the exponential stage and noticed variability in Eno localization patterns between all the three strains. Eno was found to be predominantly localized on the cell membrane in the Bas Δ prkC as compared to the Bas-wt and PrkC complement strains (Fig. 8B), indicating that the unphosphorylated isoform preferentially localizes at the membrane in vegetative cells.

In *B. subtilis*, Eno is known to be secreted via the non-classical secretion pathway through a membrane-embedded hydrophobic domain (37,38). We checked if Eno secretion could also be impacted upon phosphorylation. So, culture supernatants and cell lysates of the Bas-wt and Bas Δ prkC cells grown to the late exponential phase were subjected to immunoblotting with anti-Eno antibodies. As a control, we used a very well-known secretory protein from *B. anthracis*-the protective antigen (PA), which also forms part of the anthrax vaccine. The supernatant fraction was probed with the polyclonal antibody to PA to confirm that the supernatant contained the secreted proteins. Immunoblots showed that *B. anthracis* Eno is secreted from the cell, but secretion was independent of its phosphorylation status (Fig. 8C). Thus, we conclude that PrkC affected the localization of Eno, but not its secretion.

CONCLUSIONS

Development of spore to a vegetative cell requires a shift in metabolism. During spore formation, bacteria downregulate their metabolism by halting transcriptional and translational machinery and storing energy reserves. At the beginning of germination, a spore requires substantial metabolic supplements. PrkC is known to sense germination cues from the environment and helps in regulating translation and metabolism during the spore germination. One of the primary questions in cellular development is how the metabolic machinery switches from dormancy during sporulation to exponential growth during germination. Phenotypic memory, which is a carryover of cellular material from the mother cell to the spore, is key to germination. A critical step in this developmental program is the regulation of glycolytic enzymes that store energy reserves and balance metabolic needs when germination begins. We studied the expression of three glycolytic enzymes and identified Eno as a metabolic switch that holds the key to

germination and contributes to phenotypic memory. Our results further identified PrkC to augment the germination process by maintaining Eno quantity, localization and its enzymatic activity (Fig. 9).

In conclusion, our results provide evidence of Eno regulation by phosphorylation and its involvement in the process of germination of *B. anthracis* spores. Our study elucidates the phosphorylation of Eno and identifies its regulation by PrkC. The role of PrkC has been previously discussed in spore germination (12). Our results show that during sporulation PrkC initiates imprinting phenotypic memory by modifying the metabolic protein Eno. This imprinted memory helps *B. anthracis* to survive the nutritional shift and helps in spore germination.

EXPERIMENTAL PROCEDURES

Bacterial strains and growth conditions. *E. coli* strains DH5 α (Novagen) and BL21(DE3) (Agilent) were used for cloning and expression of recombinant proteins, respectively. *E. coli* cells were grown and maintained with constant shaking (200 rpm) at 37°C in LB broth supplemented with 100 μ g/ml ampicillin or 25 μ g/ml chloramphenicol, for the co-expression system. *B. anthracis* Sterne strains wild type (Bas-wt), PrkC deletion strain (Bas Δ prkC) and prkC-complement strains (Bas Δ prkC complement) (12), were grown in LB media supplemented with antibiotics as required. LB agar was used as the solid medium for culturing both *E. coli* and *B. anthracis* in presence of selective antibiotics.

Cloning and mutagenesis of *B. anthracis* genes. Cloning and mutagenesis were performed according to the standard molecular biology procedures described earlier using *B. anthracis* Sterne strain genomic DNA (39,40). The coding sequences of *eno* (Bas4985), *pgm* (Bas4986) and *pgk* (Bas4988) from *B. anthracis* were amplified by PCR using primers containing SpeI and BamHI restriction sites with six histidine repeat sequences in the reverse primer (Table S1). The resulting PCR product was cloned into *E. coli/B. anthracis* shuttle vector pYS5. Clones were then confirmed with restriction digestion and DNA sequencing (SciGenome). The confirmed plasmid was electroporated in *B. anthracis* Sterne strains (Bas-wt or Bas Δ prkC) using BTX Electro Cell Manipulator 600. For cloning and expression in

E. coli, *eno* was amplified by PCR using primers containing BamHI and XhoI restriction sites. The resulting PCR product was cloned in pPro-Ex-HTc. To generate the site-specific mutants of Eno, site-directed mutagenesis was performed using the Quikchange® XL Site-Directed Mutagenesis kit (Agilent).

Expression and purification of recombinant *B. anthracis* proteins. The recombinant His₆-tagged fusion proteins were over-expressed and purified from *E. coli* and *B. anthracis* as described previously (28). *E. coli* BL21-DE3 strains harboring plasmid pACYC-PrkC or pACYC-PrpC were co-transformed with Bas4985 (*eno*) containing plasmid (pProEx-HTc) to overexpress and purify phosphorylated (Eno-P) or unphosphorylated (Eno-UP), respectively. The phosphorylation status was checked by staining with Pro-Q Diamond phospho-specific stain (Molecular Probes, Life Technologies) according to manufacturer's instructions. The protein amounts were checked by SYPRO Ruby protein gel stain (Molecular Probes, Life Technologies) and Coomassie Brilliant Blue stain.

Sporulation and germination efficiency. Spores were prepared as described in the previous study (41). Different dilutions of heat-treated and non-treated spores were plated on LB agar and CFUs were counted. The sporulation efficiency was calculated as “CFU per mL (heat treated)/ CFU per mL (non-treated)” and compared with respect to Bas-wt (taken as 100%) (42). For germination efficiency, spores were diluted to OD₆₀₀=1 and heat treated at 70°C for 30 min (43). The heat-treated spores were serially diluted in deionized water, plated on LB agar (without antibiotics) and incubated at 37°C overnight. CFUs were counted and Bas-wt spore CFUs were taken as 100%. Statistical analysis was performed using parametric t-test.

Eno activity assay. The activity of His6-tagged Eno-UP and Eno-P (1 μ g) was measured using Eno colorimetric activity assay kit according to manufacturer's protocol (Biovision). Eno catalyzes the conversion of 2-PGA to PEP. The intermediate product formed, reacts with a peroxide substrate to generate color (OD 570 nm) at 25°C proportional to the Eno activity. A standard curve was generated with different dilutions of H₂O₂ and Eno activity was calculated using the formula:

$$\text{Enolase Activity} = \frac{\text{B} \times \text{Sample Dilution Factor}}{(\text{Reaction Time}) \times V}$$

where: B = Amount (nmole) of H₂O₂ generated between T_{initial} and T_{final} Reaction

$$\text{Reaction Time} = T_{\text{final}} - T_{\text{initial}} (\text{min})$$

V = sample volume (ml) added to the well

In vitro kinase assay. PrkC (1 µg) was used for *in vitro* kinase assay with Eno and its mutants (5 µg) in kinase buffer (20 mM HEPES pH 7.2, 10 mM MgCl₂ and 10 mM MnCl₂) containing 2 µCi [γ -³²P] ATP (BRIT, Hyderabad, India) at 25°C for 30 min as described previously (25).

Metabolic labeling. *E. coli* BL21-DE3 transformants harboring either pACYC-PrkC:Eno or pACYC-PrpC:Eno were used for metabolic labeling using [γ -³²P]-orthophosphoric acid as previously described (44). Extracted samples were analyzed by autoradiography using Personal Molecular Imager (PMI, BioRad).

Mass spectrometry analysis. Samples were resolved on SDS-PAGE and trypsinized to prepare peptide mixtures for mass spectrometric analysis (45). Peptides were separated and measured by LC-ESI-mass spectrometry using the Easy-nLCII HPLC system (Thermo Fisher Scientific) coupled directly to an LTQ Orbitrap VelosTM mass spectrometer (ThermoFisher Scientific). Proteins were identified by searching all MS/MS spectra against a forward-reverse database that was composed of all protein sequences of *B. anthracis* Sterne and common contaminants using SorcererTM-SEQUEST (Thermo Fisher Scientific; version v.27, rev.11) in conjunction with Scaffold (version 3 00 06, Proteome Software Inc., Portland, OR).

Immuno-electron microscopy (Immuno-EM). *B. anthracis* Sterne strain (Bas-wt), kinase deletion mutant (Bas Δ prkC) and the complemented strain (Bas Δ prkC complement) were grown at 37°C to the mid-log phase and harvested. The cells were fixed in 2% paraformaldehyde and 0.05% glutaraldehyde dissolved in 0.1 M sodium phosphate buffer (PB) (pH 7.4) for 2 h and then washed three times with PB. The cells were then resuspended in 2% agar and harvested again. The cell pellets were immersed in 30% sucrose (wt/vol) overnight at 4°C and subjected to immunolabeling as described previously (46), using 1:10 dilution of anti-Eno antibodies and the pre-immune sera as a control. Ultrathin sections

(70 nm thick) were cut on RMC ultra-microtome, stained with 1% Uranyl acetate and imaged in Tecnai G2 20 twin (FEI) transmission electron microscope. Cell surface Enolase expression was normalized with cytosolic expression using Fiji-ImageJ and plotted using GraphPad Prism

Magnesium binding assay. The unphosphorylated (Eno-UP) and phosphorylated (Eno-P) forms of Eno were used in interaction studies with MgCl₂. The reaction was initiated by the addition of the proteins (1 µM) each to fluorescence assay buffer, buffer F (1 mM PEP (Sigma), 0.1 M HEPES [pH 7], 7.7 mM KCl) with MgCl₂ (0.05 mM). A buffer containing PEP, HEPES and KCl served as control. The emission spectra were recorded from 310 nm to 430 nm after excitation at 280 nm (Fluoromax-3 spectrofluorimeter; Jobin Yvon Horiba) with an integration time of 1s. The association of MgCl₂ with Eno was measured by mixing increasing concentrations of MgCl₂ (0.05 mM to 10 mM) with 1 µM concentration of Eno (Eno-P and Eno-UP) in buffer F at 25°C. The experiment was performed by monitoring the fluorescence change over time (35).

Enzyme-Linked immunosorbent assay (ELISA). An indirect ELISA was performed as described earlier with some modifications (47). Briefly, His₆ tagged Eno (100 ng/well) was dissolved in a coating buffer (carbonate-bicarbonate buffer; pH-9.6) and adsorbed on the surface of a 96-well ELISA plate (Maxisorb, Nunc) for 16 h at 4°C. The test serum was serially diluted (1% in PBS) and added to each well to be kept for 1 h at 37°C. Pre-immune serum was used as a control. The experiment was done in triplicates and the antibody titer was expressed as the reciprocal of the end-point dilution.

Antibody generation and Western blotting. *B. anthracis* Eno (Bas4985) expressed in *E. coli* with His₆- tag was purified with up to 98% homogeneity (as per SDS PAGE analysis). The affinity purified protein was dialyzed against Phosphate buffer saline (PBS) and analyzed to be endotoxin free using a kit-based assay (Pierce). The protein was then used to immunize a group of BALB/c mice (n=3) first in combination with Freund's complete and subsequently Freund's incomplete adjuvant. After three booster doses (2 weeks apart), the mice were bled and the isolated serum was analyzed using an indirect ELISA

which showed an efficient titer against Eno. The specificity of the Western blots was determined by probing *B. anthracis* cell lysates with different dilutions of Eno serum. The antibodies recognize a 45 kDa molecular weight protein corresponding to Eno. Purified Eno from *E. coli* was taken as a positive control and GST (Glutathione-S-transferase) was used as a negative control. anti-PA antibody was used from the previous studies (41). For estimating protein size, pre-stained protein markers were used (BioRad, catalog no. 26616, 26619, 26634).

Quantification and Statistical analysis. For the radioactivity-based experiments, the autoradiograms were quantified using QuantityOne software (BioRad) and the corresponding Coomassie Brilliant blue-stained gels were quantified using Fiji- ImageJ. The normalized values were plotted using GraphPad Prism. The Western blots were quantified using Fiji-ImageJ software and the respective values normalized by the controls were plotted using GraphPad Prism. For time-dependent 2-D gel electrophoresis, the amount of phosphorylation at a given time point is calculated by employing the formula:

$$\text{Intensity of phosphorylation (at a given time point)} = (\text{the intensity of phospho-isoforms}/\text{Intensity of the total input protein}) \times 100$$

For statistical significance, parametric unpaired t-test was performed with Welch's correction.

Circular Dichroism Spectroscopy. CD spectra of Eno and its mutants (Eno-wt, Eno-UP, Eno-P, Eno-S336A/T363A/S367A) were recorded using Jasco J-815 CD spectro-polarimeter. The spectrum was recorded from 190 nm to 250 nm at 25°C using a cell of 0.1 cm path length. Experiments were repeated thrice and molar ellipticity values with respect to wavelength were analyzed using a K2D3 web server to estimate the protein secondary structure (48).

Animals ethics approval. The animal experiments were performed according to the Institutional Animal Ethics Committee (IAEC) of Defense Research and Development Establishment (registration number 37/GO/c/1999/CPCSEA dated 13.04.2011. The animals were maintained as per the approved guidelines of the committee for the purpose of Control and Supervision of Experiments on Animals (CPCSEA), Government. of India. The study was also approved by the Institutional Biosafety Committee of Defense Research and Development Establishment, DRDO, Ministry of Defense, Government of India vide protocol no. IBSC/12/BT/AKG/22. For generation of antibodies, animals were used (mice, rabbit) after approval of animal ethics committee in CSIR-Institute of Genomics and Integrative Biology.

Acknowledgements: This work was supported by J.C. Bose fellowship (SERB, DST); CSIR senior research fellowship (to R.V.). Support of Brain Pool grant (NRF-2018H1D3A2001746) by National Research Foundation of Korea (NRF) to VCK to work at Konkuk University and Basic Science Research Program of NRF funded by the Ministry of Science, ICT & Future Planning (2017R1A2B3011676, 2017R1A4A1014806, 2013M3A6A8073184) to JKL is acknowledged. We thank NIH Fellows Editorial Board, Kriti Arora and Abhinav Kumar for help in manuscript editing.

Conflict of interest: The authors declare that they have no conflicts of interest with the contents of this article.

REFERENCES

1. Arora, G., Misra, R., and Sajid, A. (2017) Model Systems for Pulmonary Infectious Diseases: Paradigms of Anthrax and Tuberculosis. *Curr Top Med Chem* **17**, 2077-2099
2. Beyer, W., and Turnbull, P. C. (2009) Anthrax in animals. *Mol Aspects Med* **30**, 481-489
3. Errington, J. (2003) Regulation of endospore formation in *Bacillus subtilis*. *Nat Rev Microbiol* **1**, 117-126
4. Zheng, L., Abhyankar, W., Ouwerling, N., Dekker, H. L., van Veen, H., van der Wel, N. N., Roseboom, W., de Koning, L. J., Brul, S., and de Koster, C. G. (2016) *Bacillus subtilis* Spore Inner Membrane Proteome. *J Proteome Res* **15**, 585-594
5. Sinai, L., Rosenberg, A., Smith, Y., Segev, E., and Ben-Yehuda, S. (2015) The molecular timeline of a reviving bacterial spore. *Mol Cell* **57**, 695-707
6. Segev, E., Smith, Y., and Ben-Yehuda, S. (2012) RNA dynamics in aging bacterial spores. *Cell* **148**, 139-149
7. Mutlu, A., Trauth, S., Ziesack, M., Nagler, K., Bergeest, J. P., Rohr, K., Becker, N., Hofer, T., and Bischofs, I. B. (2018) Phenotypic memory in *Bacillus subtilis* links dormancy entry and exit by a spore quantity-quality tradeoff. *Nat Commun* **9**, 69
8. Kuijper, B., and Johnstone, R. A. (2016) Parental effects and the evolution of phenotypic memory. *J Evol Biol* **29**, 265-276
9. Wang, S., Faeder, J. R., Setlow, P., and Li, Y. Q. (2015) Memory of Germinant Stimuli in Bacterial Spores. *MBio* **6**, e01859-01815
10. Pereira, S. F., Gonzalez, R. L., Jr., and Dworkin, J. (2015) Protein synthesis during cellular quiescence is inhibited by phosphorylation of a translational elongation factor. *Proc Natl Acad Sci U S A* **112**, E3274-3281
11. Setlow, P. (2014) Germination of spores of *Bacillus* species: what we know and do not know. *J Bacteriol* **196**, 1297-1305
12. Shah, I. M., Laaberki, M. H., Popham, D. L., and Dworkin, J. (2008) A eukaryotic-like Ser/Thr kinase signals bacteria to exit dormancy in response to peptidoglycan fragments. *Cell* **135**, 486-496
13. Korza, G., Setlow, B., Rao, L., Li, Q., and Setlow, P. (2016) Changes in *Bacillus* Spore Small Molecules, rRNA, Germination, and Outgrowth after Extended Sublethal Exposure to Various Temperatures: Evidence that Protein Synthesis Is Not Essential for Spore Germination. *J Bacteriol* **198**, 3254-3264
14. Commichau, F. M., Rothe, F. M., Herzberg, C., Wagner, E., Hellwig, D., Lehnik-Habrink, M., Hammer, E., Volker, U., and Stulke, J. (2009) Novel activities of glycolytic enzymes in *Bacillus subtilis*: interactions with essential proteins involved in mRNA processing. *Mol Cell Proteomics* **8**, 1350-1360
15. Ghosh, S., Korza, G., Maciejewski, M., and Setlow, P. (2015) Analysis of metabolism in dormant spores of *Bacillus* species by 31P nuclear magnetic resonance analysis of low-molecular-weight compounds. *J Bacteriol* **197**, 992-1001
16. Sunde, E. P., Setlow, P., Hederstedt, L., and Halle, B. (2009) The physical state of water in bacterial spores. *Proc Natl Acad Sci U S A* **106**, 19334-19339
17. Leyva-Vazquez, M. A., and Setlow, P. (1994) Cloning and nucleotide sequences of the genes encoding triose phosphate isomerase, phosphoglycerate mutase, and enolase from *Bacillus subtilis*. *J Bacteriol* **176**, 3903-3910
18. Setlow, P., and Kornberg, A. (1970) Biochemical studies of bacterial sporulation and germination. XXII. Energy metabolism in early stages of germination of *Bacillus megaterium* spores. *J Biol Chem* **245**, 3637-3644
19. Agarwal, S., Kulshreshtha, P., Bambah Mukku, D., and Bhatnagar, R. (2008) alpha-Enolase binds to human plasminogen on the surface of *Bacillus anthracis*. *Biochim Biophys Acta* **1784**, 986-994

20. Kudva, I. T., Griffin, R. W., Garren, J. M., Calderwood, S. B., and John, M. (2005) Identification of a protein subset of the anthrax spore immunome in humans immunized with the anthrax vaccine adsorbed preparation. *Infect Immun* **73**, 5685-5696
21. Sajid, A., Arora, G., Singhal, A., Kalia, V. C., and Singh, Y. (2015) Protein Phosphatases of Pathogenic Bacteria: Role in Physiology and Virulence. *Annu Rev Microbiol* **69**, 527-547
22. Bryant-Hudson, K. M., Shakir, S. M., and Ballard, J. D. (2011) Autoregulatory characteristics of a *Bacillus anthracis* serine/threonine kinase. *J Bacteriol* **193**, 1833-1842
23. Pompeo, F., Foulquier, E., and Galinier, A. (2016) Impact of Serine/Threonine Protein Kinases on the Regulation of Sporulation in *Bacillus subtilis*. *Front Microbiol* **7**, 568
24. Setlow, P. (2008) Dormant spores receive an unexpected wake-up call. *Cell* **135**, 410-412
25. Arora, G., Sajid, A., Arulanandh, M. D., Singhal, A., Mattoo, A. R., Pomerantsev, A. P., Leppla, S. H., Maiti, S., and Singh, Y. (2012) Unveiling the novel dual specificity protein kinases in *Bacillus anthracis*: identification of the first prokaryotic dual specificity tyrosine phosphorylation-regulated kinase (DYRK)-like kinase. *J Biol Chem* **287**, 26749-26763
26. Arora, G., Sajid, A., Gupta, M., Bhaduri, A., Kumar, P., Basu-Modak, S., and Singh, Y. (2010) Understanding the role of PknJ in *Mycobacterium tuberculosis*: biochemical characterization and identification of novel substrate pyruvate kinase A. *PLoS One* **5**, e10772
27. Rosenberg, A., Soufi, B., Ravikumar, V., Soares, N. C., Krug, K., Smith, Y., Macek, B., and Ben-Yehuda, S. (2015) Phosphoproteome dynamics mediate revival of bacterial spores. *BMC Biol* **13**, 76
28. Arora, G., Sajid, A., Virmani, R., Singhal, A., Kumar, C. M. S., Dhasmana, N., Khanna, T., Maji, A., Misra, R., Molle, V., Becher, D., Gerth, U., Mande, S. C., and Singh, Y. (2017) Ser/Thr protein kinase PrkC-mediated regulation of GroEL is critical for biofilm formation in *Bacillus anthracis*. *NPJ Biofilms Microbiomes* **3**, 7
29. Newman, J. A., Hewitt, L., Rodrigues, C., Solovyova, A. S., Harwood, C. R., and Lewis, R. J. (2012) Dissection of the network of interactions that links RNA processing with glycolysis in the *Bacillus subtilis* degradosome. *J Mol Biol* **416**, 121-136
30. Schreier, B., and Hocker, B. (2010) Engineering the enolase magnesium II binding site: implications for its evolution. *Biochemistry* **49**, 7582-7589
31. Boel, G., Pichereau, V., Mijakovic, I., Maze, A., Poncet, S., Gillet, S., Giard, J. C., Hartke, A., Auffray, Y., and Deutscher, J. (2004) Is 2-phosphoglycerate-dependent automodification of bacterial enolases implicated in their export? *J Mol Biol* **337**, 485-496
32. Leggett, M. J., McDonnell, G., Denyer, S. P., Setlow, P., and Maillard, J. Y. (2012) Bacterial spore structures and their protective role in biocide resistance. *J Appl Microbiol* **113**, 485-498
33. Granger, A. C., Gaidamakova, E. K., Matrosova, V. Y., Daly, M. J., and Setlow, P. (2011) Effects of Mn and Fe levels on *Bacillus subtilis* spore resistance and effects of Mn²⁺, other divalent cations, orthophosphate, and dipicolinic acid on protein resistance to ionizing radiation. *Appl Environ Microbiol* **77**, 32-40
34. Lebioda, L., and Stec, B. (1991) Mechanism of enolase: the crystal structure of enolase-Mg2(+)-2-phosphoglycerate/phosphoenolpyruvate complex at 2.2-A resolution. *Biochemistry* **30**, 2817-2822
35. Gao, X., Tang, Y., Rong, W., Zhang, X., Zhao, W., and Zi, Y. (2011) Analysis of binding interaction between captopril and human serum albumin. *American Journal of Analytical Chemistry* **2**, 250-257
36. Shakir, S. M., Bryant, K. M., Larabee, J. L., Hamm, E. E., Lovchik, J., Lyons, C. R., and Ballard, J. D. (2010) Regulatory interactions of a virulence-associated serine/threonine phosphatase-kinase pair in *Bacillus anthracis*. *J Bacteriol* **192**, 400-409
37. Yang, C. K., Zhang, X. Z., Lu, C. D., and Tai, P. C. (2014) An internal hydrophobic helical domain of *Bacillus subtilis* enolase is essential but not sufficient as a non-cleavable signal for its secretion. *Biochem Biophys Res Commun* **446**, 901-905
38. Yang, C. K., Ewis, H. E., Zhang, X., Lu, C. D., Hu, H. J., Pan, Y., Abdelal, A. T., and Tai, P. C. (2011) Nonclassical protein secretion by *Bacillus subtilis* in the stationary phase is not due to cell lysis. *J Bacteriol* **193**, 5607-5615
39. Singhal, A., Arora, G., Virmani, R., Kundu, P., Khanna, T., Sajid, A., Misra, R., Joshi, J., Yadav, V., Samanta, S., Saini, N., Pandey, A. K., Visweswariah, S. S., Hentschker, C., Becher,

- D., Gerth, U., and Singh, Y. (2015) Systematic Analysis of Mycobacterial Acylation Reveals First Example of Acylation-mediated Regulation of Enzyme Activity of a Bacterial Phosphatase. *J Biol Chem* **290**, 26218-26234
40. Arora, G., Sajid, A., Arulanandh, M. D., Misra, R., Singhal, A., Kumar, S., Singh, L. K., Mattoo, A. R., Raj, R., Maiti, S., Basu-Modak, S., and Singh, Y. (2013) Zinc regulates the activity of kinase-phosphatase pair (BasPrkC/BasPrpC) in *Bacillus anthracis*. *Biometals* **26**, 715-730
41. Singh, L. K., Dhasmana, N., Sajid, A., Kumar, P., Bhaduri, A., Bharadwaj, M., Gandotra, S., Kalia, V. C., Das, T. K., Goel, A. K., Pomerantsev, A. P., Misra, R., Gerth, U., Leppla, S. H., and Singh, Y. (2015) clpC operon regulates cell architecture and sporulation in *Bacillus anthracis*. *Environ Microbiol* **17**, 855-865
42. Dale, J. L., Raynor, M. J., Ty, M. C., Hadjifrangiskou, M., and Koehler, T. M. (2018) A Dual Role for the *Bacillus anthracis* Master Virulence Regulator AtxA: Control of Sporulation and Anthrax Toxin Production. *Front Microbiol* **9**, 482
43. Paidhungat, M., and Setlow, P. (2000) Role of ger proteins in nutrient and nonnutritive triggering of spore germination in *Bacillus subtilis*. *J Bacteriol* **182**, 2513-2519
44. Singhal, A., Arora, G., Sajid, A., Maji, A., Bhat, A., Virmani, R., Upadhyay, S., Nandicoori, V. K., Sengupta, S., and Singh, Y. (2013) Regulation of homocysteine metabolism by *Mycobacterium tuberculosis* S-adenosylhomocysteine hydrolase. *Sci Rep* **3**, 2264
45. Schmidl, S. R., Gronau, K., Pietack, N., Hecker, M., Becher, D., and Stulke, J. (2010) The phosphoproteome of the minimal bacterium *Mycoplasma pneumoniae*: analysis of the complete known Ser/Thr kinase suggests the existence of novel kinases. *Mol Cell Proteomics* **9**, 1228-1242
46. Melo, R. C., Morgan, E., Monahan-Earley, R., Dvorak, A. M., and Weller, P. F. (2014) Pre-embedding immunogold labeling to optimize protein localization at subcellular compartments and membrane microdomains of leukocytes. *Nat Protoc* **9**, 2382-2394
47. Arora, G., Sajid, A., Singhal, A., Joshi, J., Virmani, R., Gupta, M., Verma, N., Maji, A., Misra, R., Baronian, G., Pandey, A. K., Molle, V., and Singh, Y. (2014) Identification of Ser/Thr kinase and forkhead associated domains in *Mycobacterium ulcerans*: characterization of novel association between protein kinase Q and MupFHA. *PLoS Negl Trop Dis* **8**, e3315
48. Louis-Jeune, C., Andrade-Navarro, M. A., and Perez-Iratxeta, C. (2012) Prediction of protein secondary structure from circular dichroism using theoretically derived spectra. *Proteins* **80**, 374-381

Table 1: Kinetic Parameters of Circular Dichroism analysis.

Parameters	Eno-wt	Eno^{S336A/T363A/S367A}	Eno-P	Eno-UP
Alpha Helix (%)	71.56	69.91	69.84	70.85
Beta Strand (%)	5.06	5.13	5.18	4.88

Figure 1

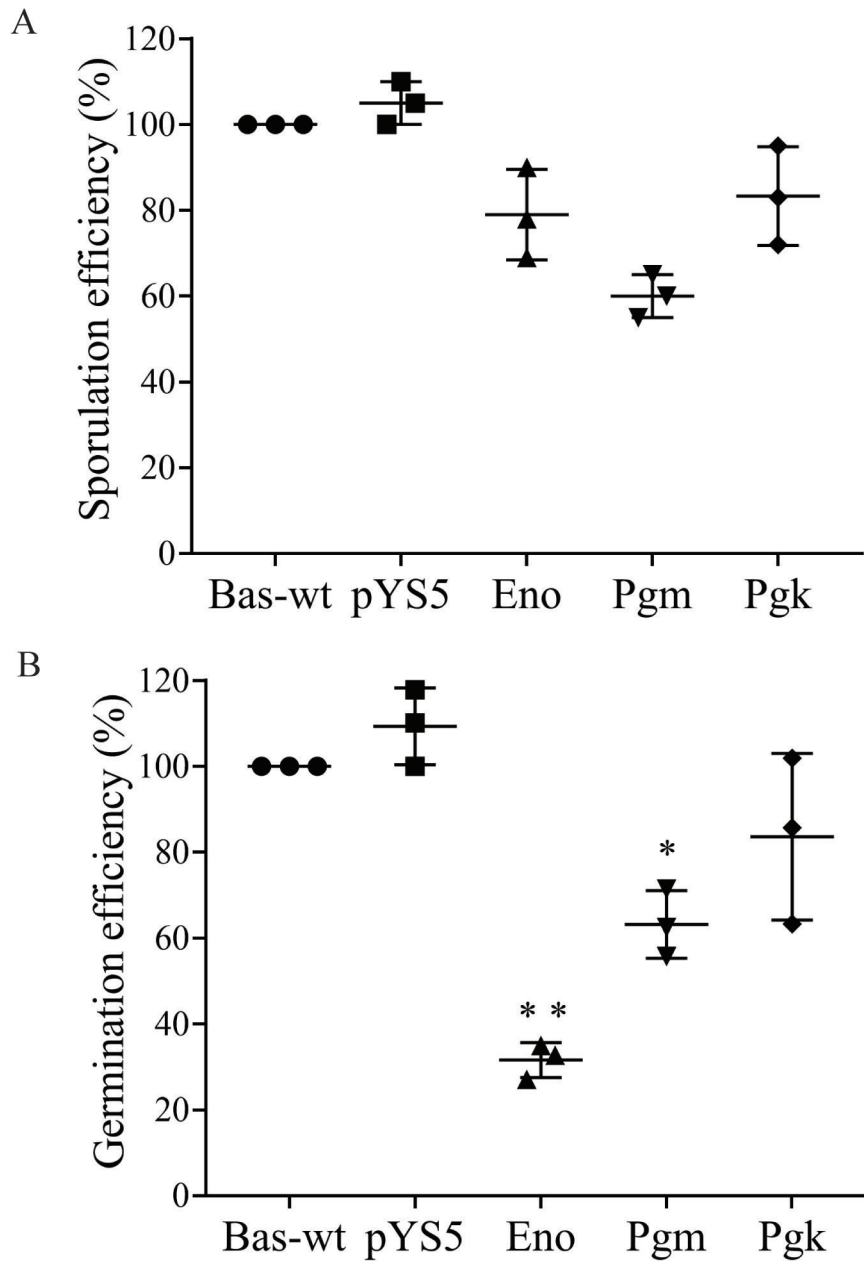


Figure 1. Role of Eno in spore germination. The bacterial strains Bas-wt, or Bas over-expressing desired gene (Eno, Pgm, Pgk and pYS5 vector control), were used for spore formation, followed by the addition of nutrient-rich medium for germination. Sporulation (A) and germination (B) efficiencies were calculated considering the efficiency of Bas-wt as 100% and plotted using GraphPad Prism. Error bars represent SD of three independent experiments. * $P \leq 0.05$, ** $P \leq 0.01$ as determined by two-tailed unpaired Student's t-test.

Figure 2

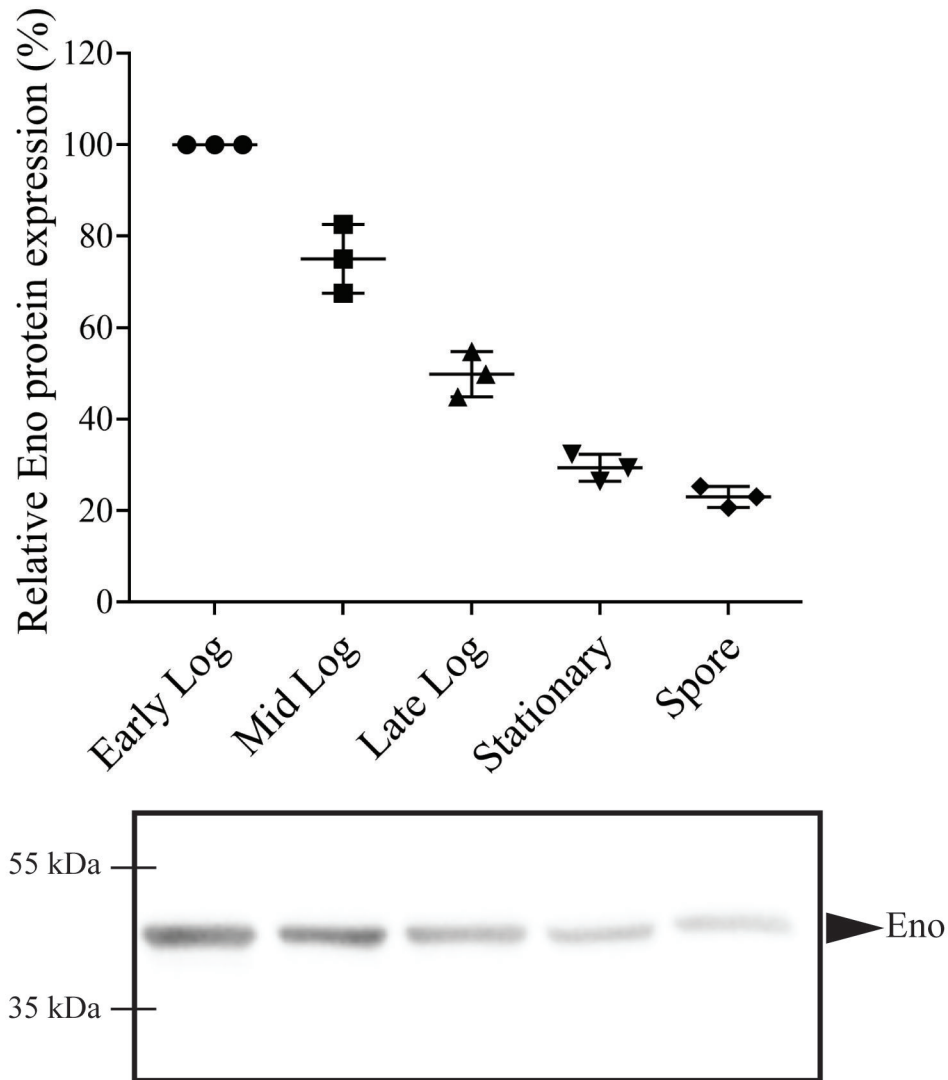


Figure 2. Decreased expression of Eno in *B. anthracis* spores. Expression analysis of Eno by immunoblotting of lysates of different growth phases [early log ($OD_{600}=0.2-0.3$), log-phase ($OD_{600} = 0.8-1.0$), late log ($OD_{600} = 1.5-1.7$) and stationary phase ($OD_{600} > 2.2$)] and spore with anti-Eno antibody. Histogram (upper panel) shows relative expression of Eno which was calculated taking the expression of Eno in early log phase as 100% in corresponding representative blot image (lower panel). Error bars represent SD of three independent experiments.

Figure 3

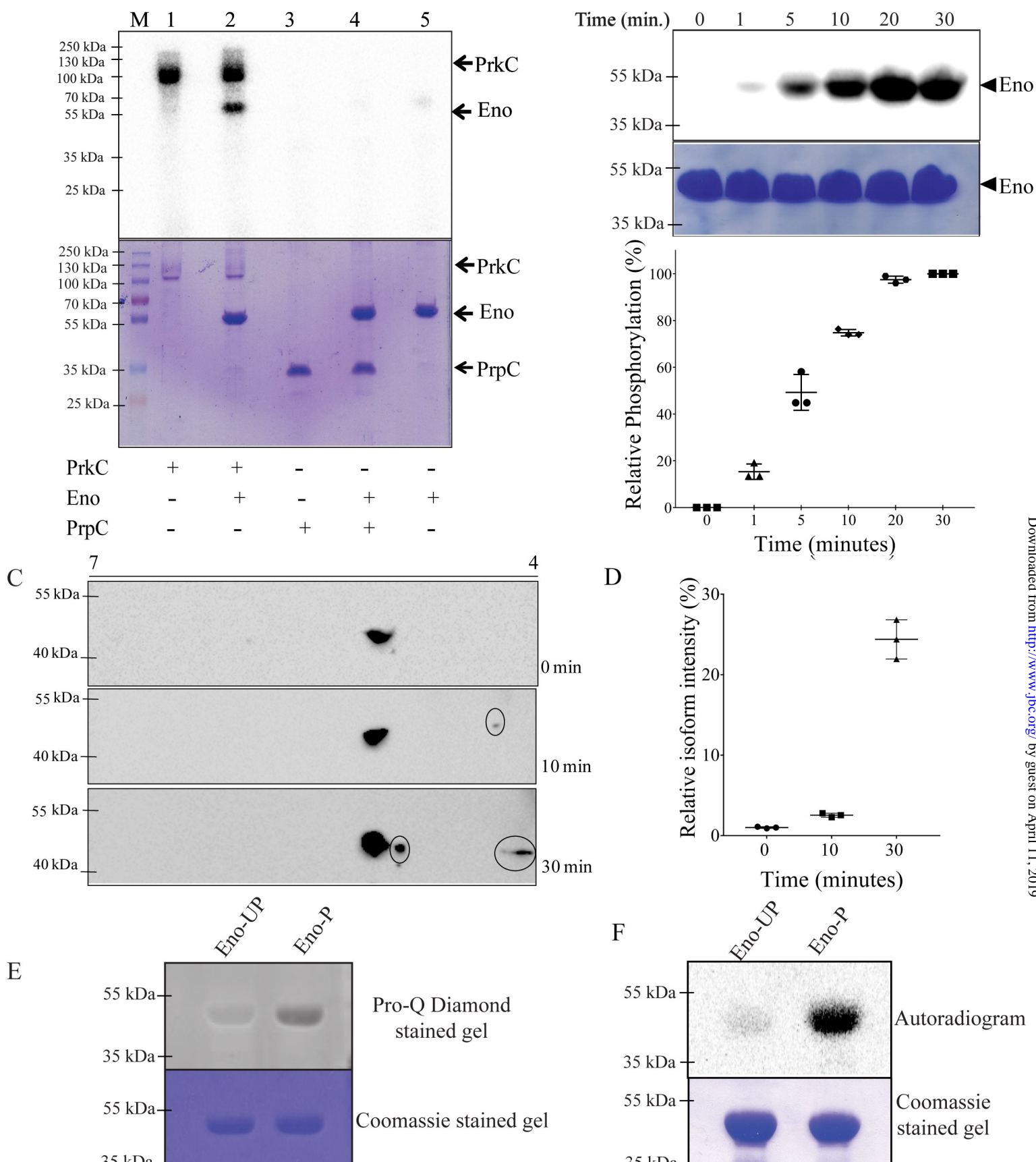
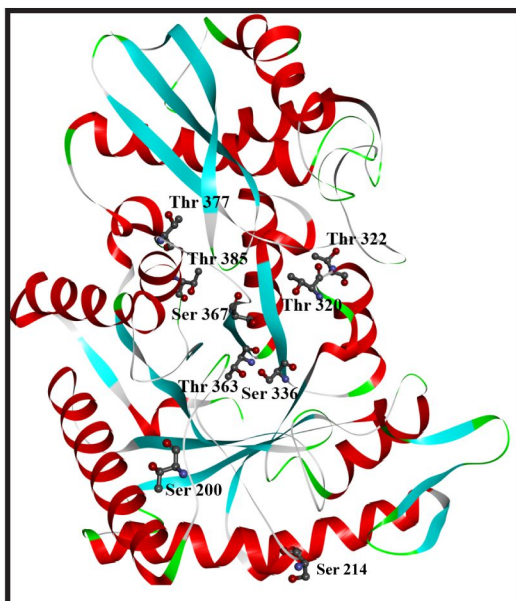


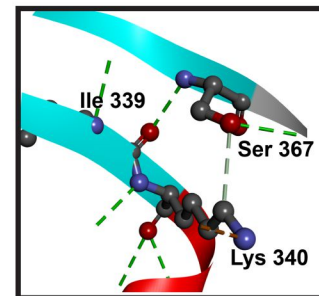
Figure 3. Eno is phosphorylated by PrkC in vitro. (A) Autoradiogram (upper panel) showing phosphorylation of recombinant Eno (5 µg) by PrkC (1 µg). PrpC (1 µg) and Eno alone were used as negative controls. The corresponding SDS-PAGE is shown (lower panel). (B) Autoradiogram showing time-dependent phosphorylation of Eno (top panel, normalized to protein amounts, lower panel) was plotted using GraphPad Prism. The intensity of phosphorylation of protein bands was calculated using QuantityOne software (BioRad). Eno phosphorylation after 30 min was taken as 100% (signal saturation) and relative phosphorylation was calculated. The error bars show SD of three independent experiments. (C and D) Time-dependent phosphorylation of Eno by PrkC using cold ATP. Isoforms were resolved by 2D-gel electrophoresis and subsequent blots were probed with anti-Eno antibodies to determine the stoichiometry of Eno phosphorylation at different time points. Multiple species (encircled) were observed after 30 min of the reaction as compared to 0 min and 10 min whose relative intensity was calculated and plotted using GraphPad Prism. (E and F) His-Eno purified from *E. coli* cells expressing Eno with PrkC (Eno-P) or PrpC (Eno-UP) were resolved by SDS-PAGE and stained with Pro-Q Diamond followed by analysis using Typhoon imager (E). *E. coli* cells over-expressing Eno-P or Eno-UP were subjected to metabolic labeling using [³²P]-orthophosphoric acid (F). In both panels, Eno-P was found to be phosphorylated whereas no phosphorylation was observed on Eno-UP.

Figure 4

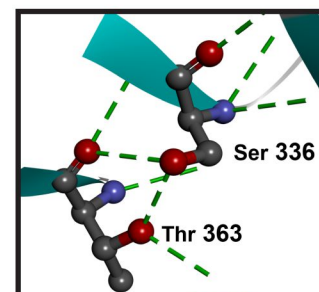
A



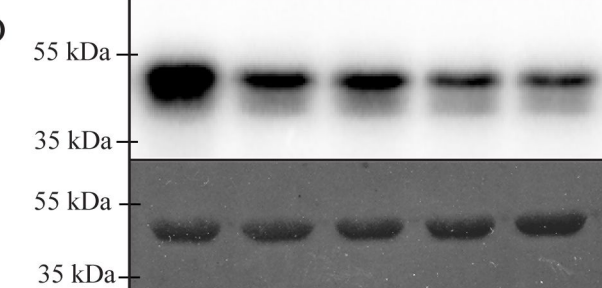
B



C

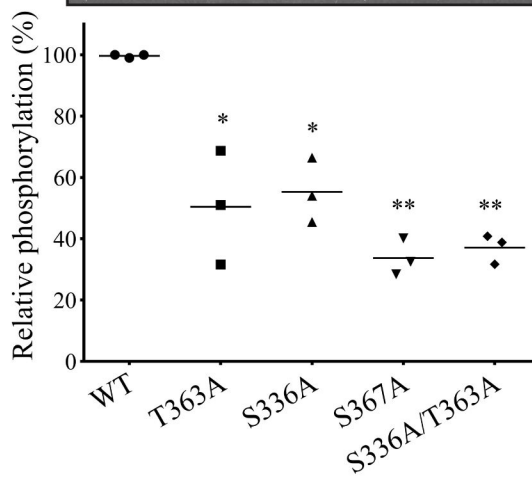


D

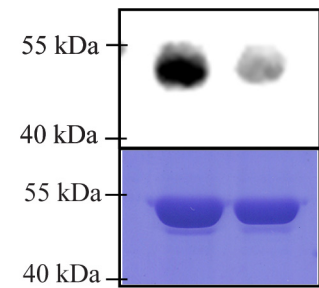


Autoradiogram

Coomassie
stained gel

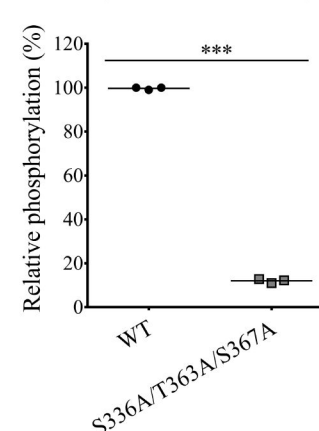


E

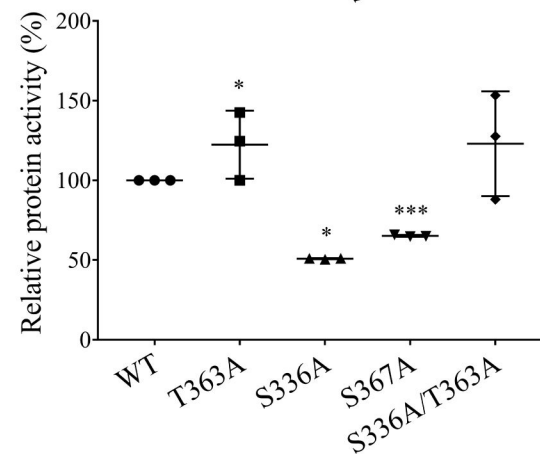


Autoradiogram

Coomassie
stained gel



F



G

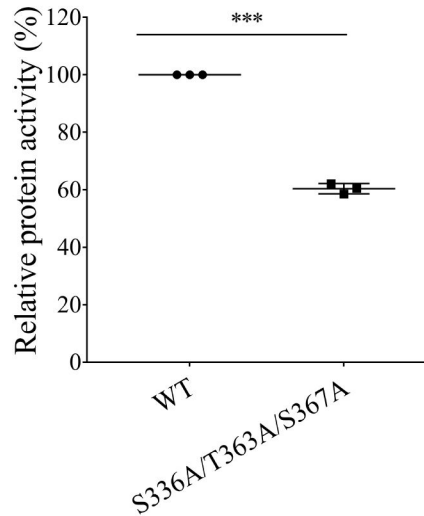


Figure 4. Mapping of the Eno phosphorylation sites. (A) Cartoon representation of the homology model of Eno from *B. anthracis*, generated using coordinates of the crystal structure of Eno from *B. subtilis* (PDB:4A3R). Helices are colored red and sheets are colored cyan. The phosphorylation sites of Eno-P, as identified by mass spectrometry, are indicated using the ball-and-stick model and are labeled. Six Thr residues (T200, T320, T322, T363, T377 and T385) and three Ser residues (S214, S336 and S367) were identified. (B and C) Residues -Ser 336, 367 and Thr363, which are evaluated in panel (D, F) are shown. Green dashed lines indicate H-bonds. (D and E) Non-phosphorylatable mutants of Eno (Ser/Thr to Ala) were assessed for their phosphorylation extent relative to the native Eno (100%). The *in vitro* kinase assay of PrkC with mutants was analyzed by autoradiogram (upper panel) and quantified by QuantityOne (lower panel). (F and G) Relative activity of Eno mutants with respect to the native Eno (100%). Native Eno is named as WT and mutants are named with respective mutation sites. All experiments were performed thrice, and error bars represent SE of three independent values. * $P \leq 0.05$, ** $P \leq 0.01$, *** $P \leq 0.001$, as determined by two-tailed unpaired Student's t-test.

Figure 5

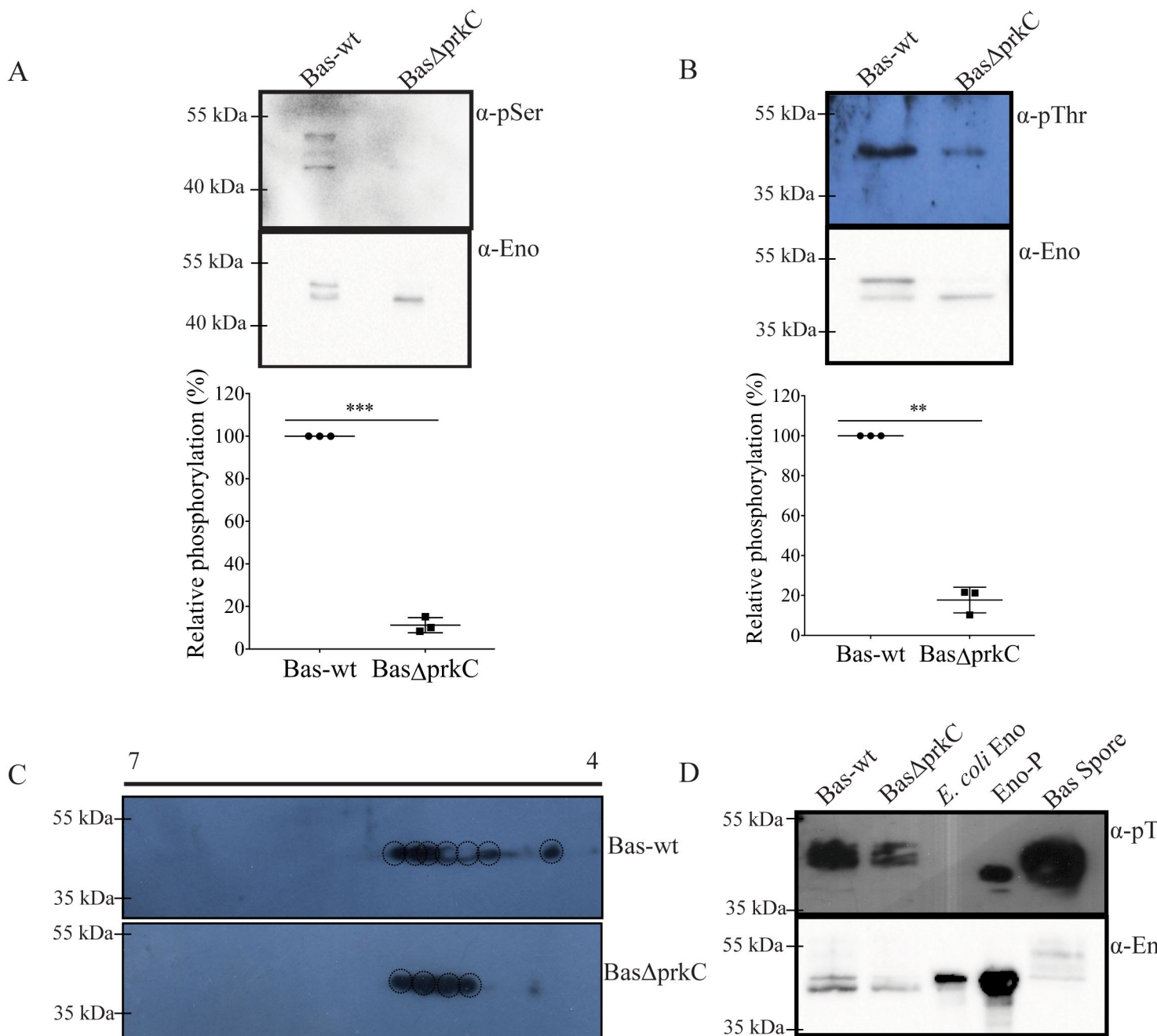


Figure 5. Phosphorylation of Eno in *B. anthracis* vegetative cells and spores. (A, B and D) Bas-Eno was over-expressed and purified from Bas-wt, Bas Δ prkC and Bas-wt spores. The protein was resolved using SDS-PAGE and probed with anti-phosphoserine and anti-phosphothreonine antibody. The blots were normalized by re-probing the blot with anti-Eno antibody. (C) The cell lysates of Bas-wt and Bas Δ prkC strain were subjected to 2D-gel electrophoresis and probed with anti-Eno antibodies to see the stoichiometry of native Eno phosphorylation. Multiple species were observed in Bas-wt lysates as compared to Bas Δ prkC which shows Eno phosphorylation by PrkC. ** $P \leq 0.01$, *** $P \leq 0.001$ as determined by two-tailed unpaired Student's t-test.

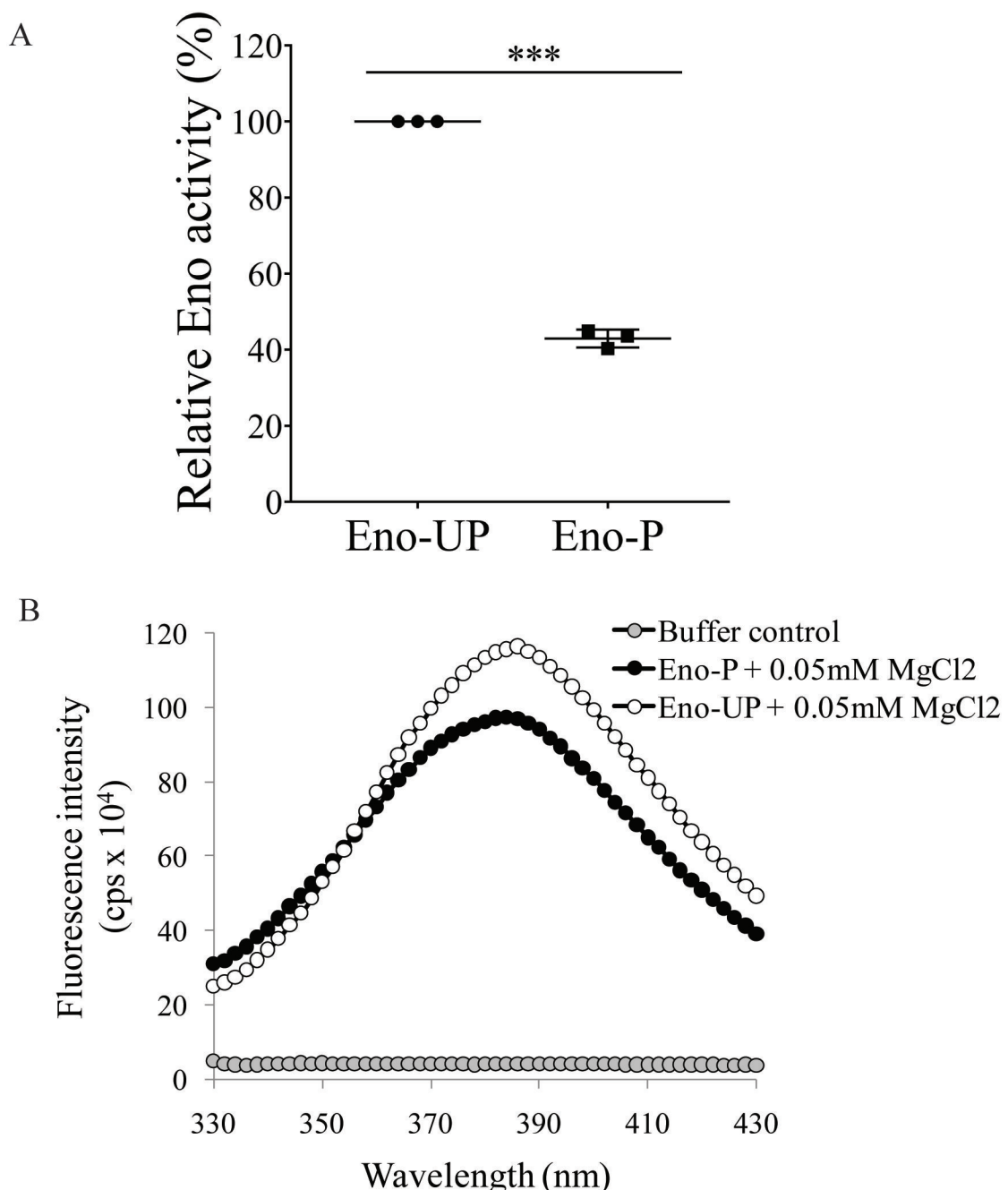
Figure 6

Figure 6. Effect of phosphorylation on Eno activity. (A) Histogram showing the comparative activity of Eno-P and Eno-UP. Phosphorylated and unphosphorylated forms were compared in identical conditions. The activity was calculated taking Eno-UP as 100%. The experiments were performed thrice and the error bars show SD of three values. (B) The interaction of Eno-P and Eno-UP (1 μ M each) with $MgCl_2$ (0.05 mM) was recorded from 330 nm to 430 nm after excitation at 280 nm. *** $P \leq 0.001$ as determined by two-tailed unpaired Student's t-test.

Figure 7

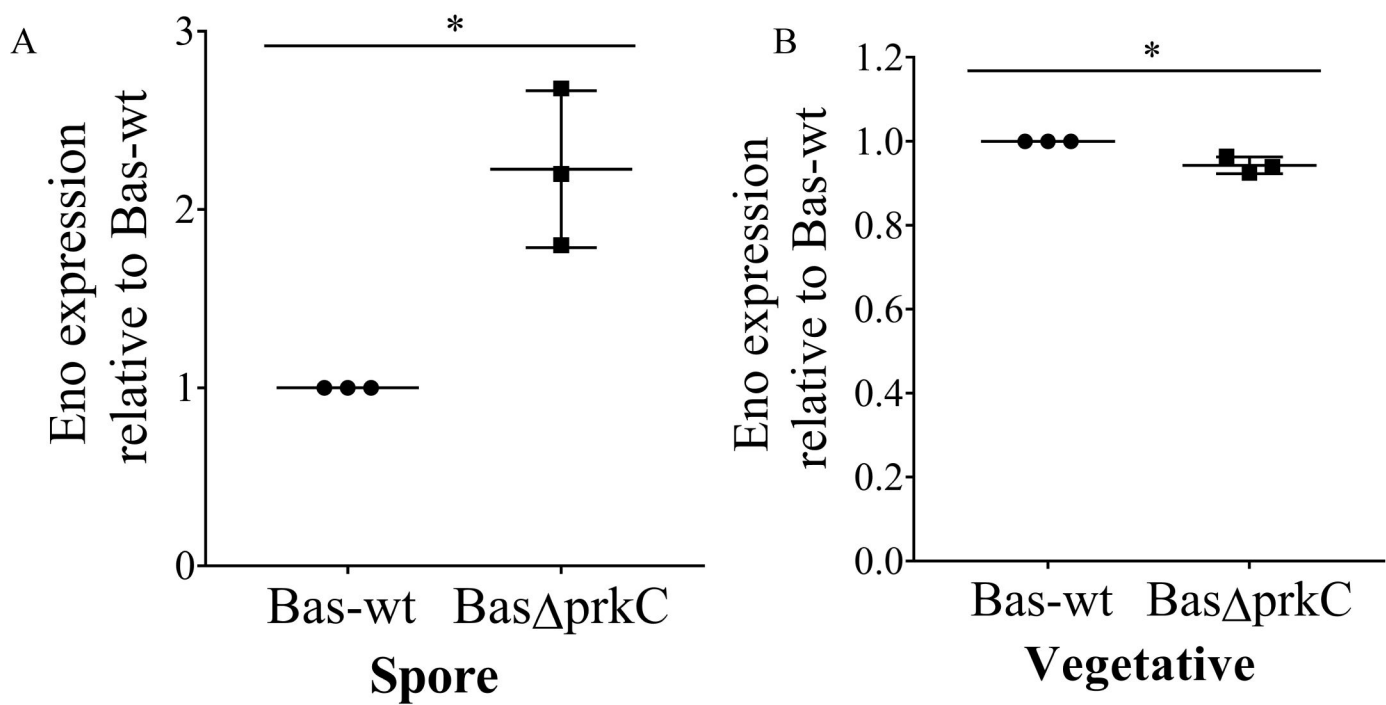
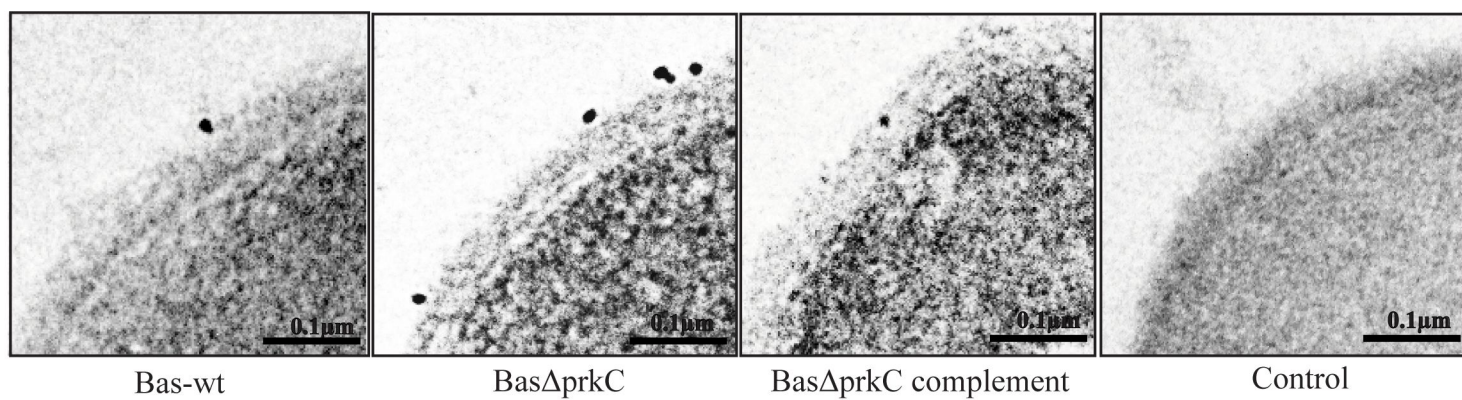


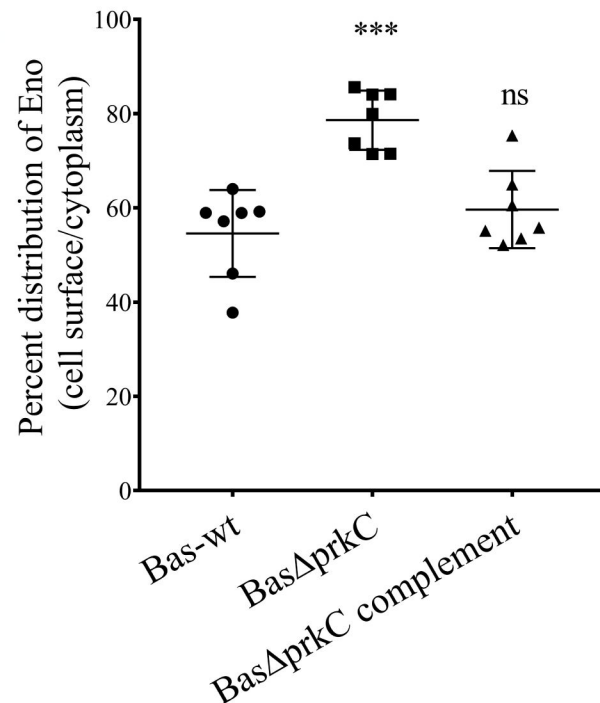
Figure 7. Relative expression of Eno. Eno expression was analyzed by comparing the spore lysates (A) and vegetative cell lysates (exponential phase) (B) of Bas-wt and prkC deletion (BasΔprkC) strains. Expression level was calculated using the Western blots (Figure S6) by Fiji-ImageJ, representing mean with SD of three independent values. * $P \leq 0.05$ as determined by two-tailed unpaired Student's t-test.

Figure 8

A



B



C

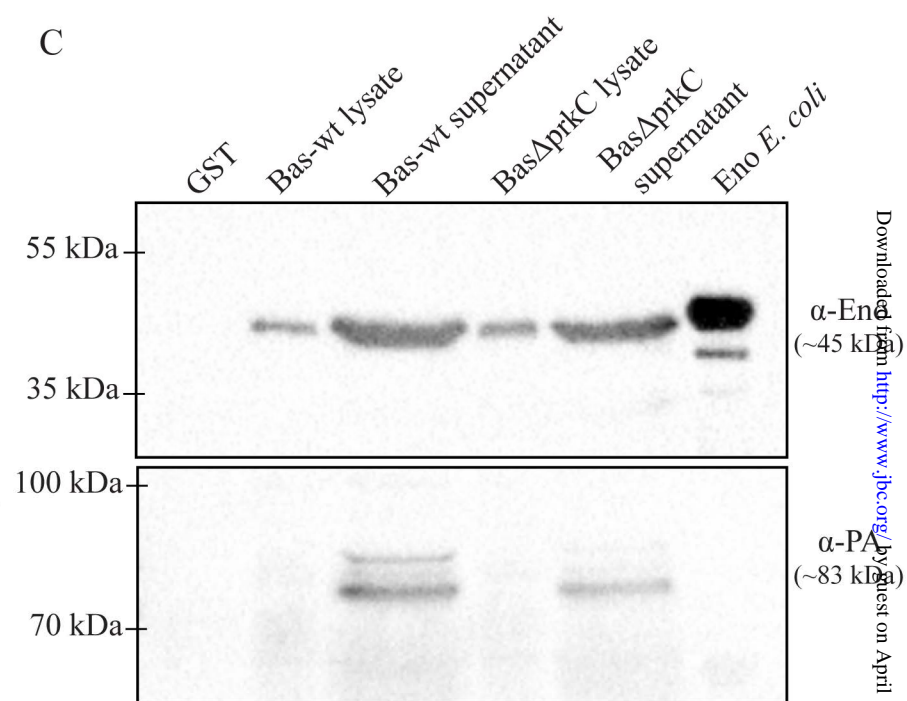


Figure 8. Localization and secretion of Eno in *B. anthracis*. (A and B) Quantitative analysis of surface localization of Eno in Bas-wt, Bas Δ prkC and Bas Δ prkC complement strains using anti-Eno (A), by counting the gold particles on the bacterial cell surface (n=7) using Fiji- ImageJ. Pre-immune serum was used as a negative control. A section is shown for immuno-EM, the full image is also provided in figure S7. (C) Lysates and secretory fraction from Bas-wt and Bas Δ prkC were subjected to immunoblotting using anti-Eno antibody (upper panel) and normalized by re-probing with anti-PA (for normalization). ***P \leq 0.001, as determined by two-tailed unpaired Student's t-test.

Figure 9

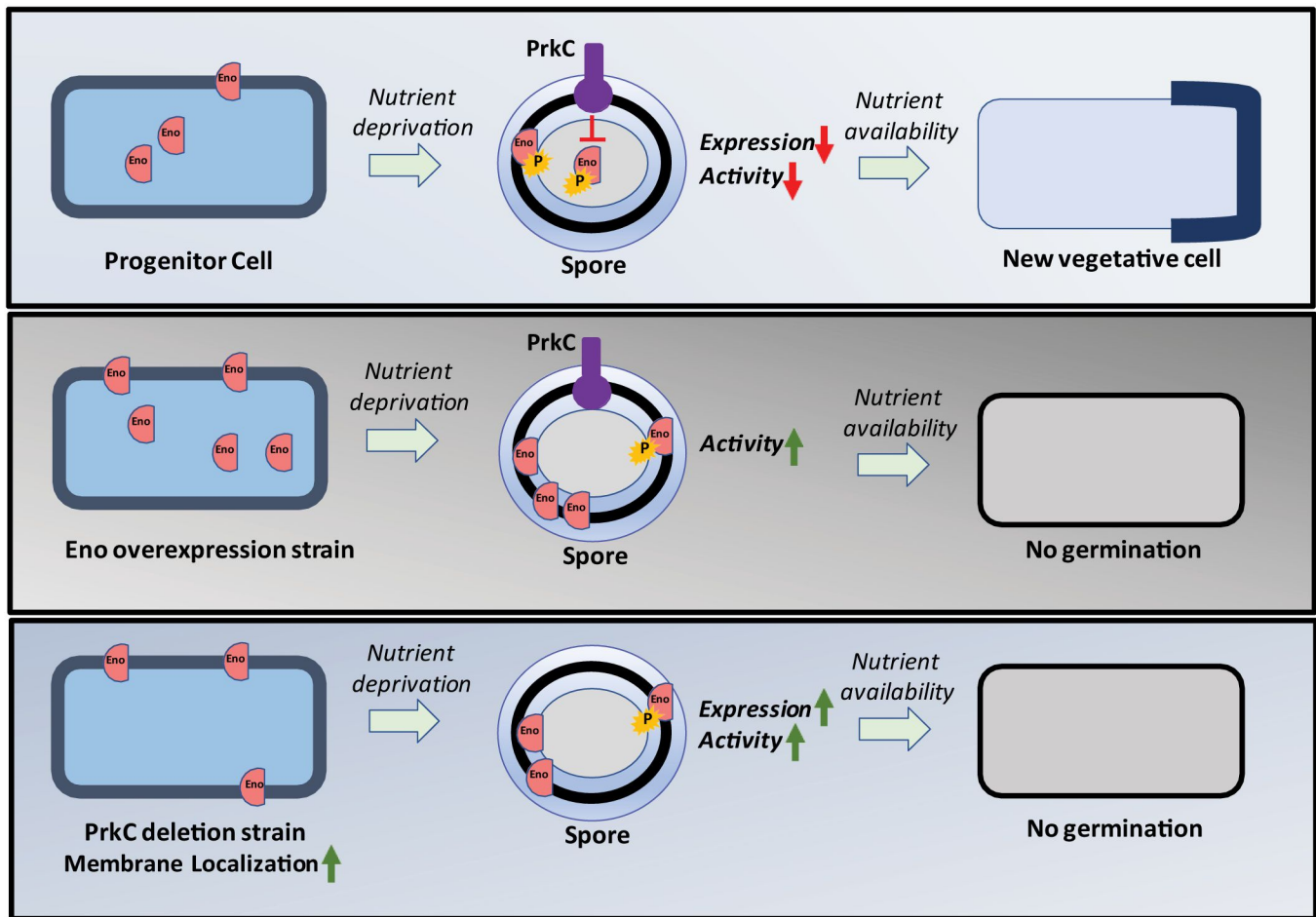


Figure 9. Proposed model illustrating PrkC and Eno interactions. The interactions are shown in native *B. anthracis*, *B. anthracis* overexpressing Eno and *B. anthracis* PrkC deficient strains and their impact on bacterial spore germination. 1) Native Eno expression- In Bas-wt cells, there is a basal level expression of Eno in vegetative cells which is carried over in the spores. The expression and activity is kept low by PrkC through phosphorylation so that the spores can germinate effectively. 2) Eno overexpression strain- The expression is raised to 1.5-fold in this strain with subsequent activation in the spore leading to spore germination defect. 3) PrkC deficient strain- Membrane localized unphosphorylated Eno is carried over in spores with increased expression and activity leading to spore germination defect.

The Ser/Thr protein kinase PrkC imprints phenotypic memory in *Bacillus anthracis* spores by phosphorylating the glycolytic enzyme enolase

Richa Virmani, Andaleeb Sajid, Anshika Singhal, Mohita Gaur, Jayadev Joshi, Ankur Bothra, Richa Garg, Richa Misra, Vijay Pal Singh, Virginie Molle, Ajay K Goel, Archana Singh, Vipin C Kalia, Jung-Kul Lee, Yasha Hasija, Gunjan Arora and Yogendra Singh

J. Biol. Chem. published online April 5, 2019

Access the most updated version of this article at doi: [10.1074/jbc.RA118.005424](https://doi.org/10.1074/jbc.RA118.005424)

Alerts:

- [When this article is cited](#)
- [When a correction for this article is posted](#)

[Click here](#) to choose from all of JBC's e-mail alerts